

Flow4R: Unifying 4D Reconstruction and Tracking with Scene Flow

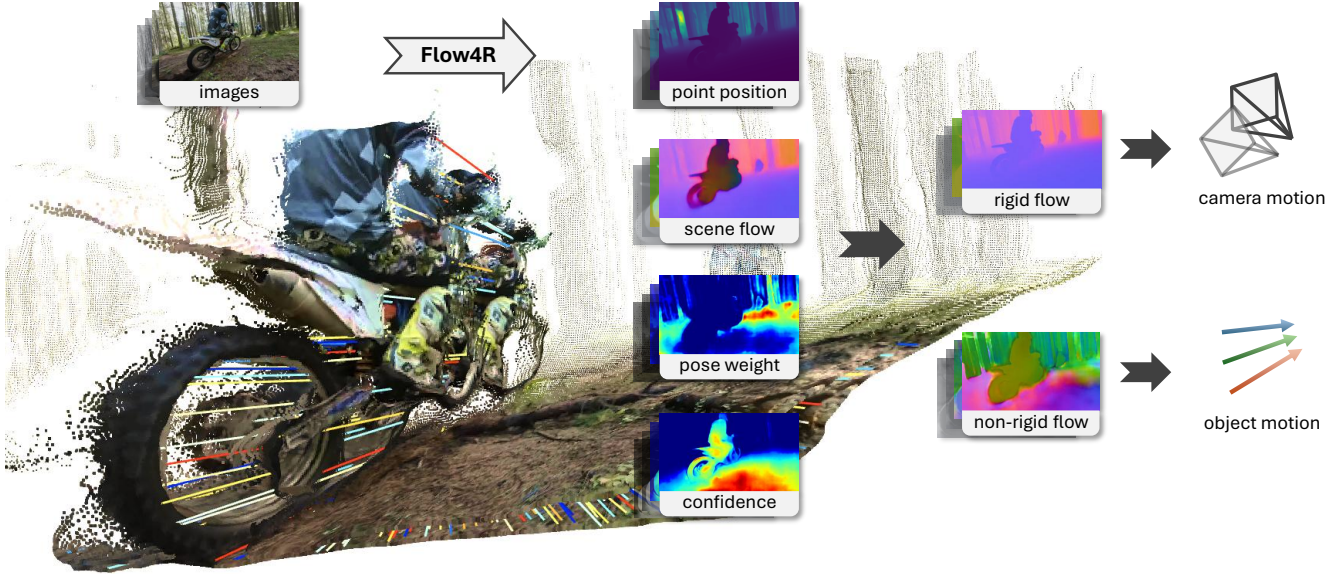
Shenhan Qian^{1,2}Ganlin Zhang^{1,2}Shangzhe Wu³Daniel Cremers^{1,2}¹Technical University of Munich ²MCML ³University of Cambridge

Figure 1. Given each image pair, Flow4R predicts for each image the point position \mathbf{P} , scene flow \mathbf{F} , pose weight \mathbf{W} , and confidence \mathbf{C} . Central to our framework, the scene flow \mathbf{F} captures motion of points relative to the camera, thus is independent of the choice of coordinate system. Based on the pose weight \mathbf{W} , the scene flow \mathbf{F} can be accurately decomposed into camera motion and object motion, enabling stable reconstruction and flexible tracking in both static and dynamic scenarios.

Abstract

Reconstructing and tracking dynamic 3D scenes remains a fundamental challenge in computer vision. Existing approaches often decouple geometry from motion: multi-view reconstruction methods assume static scenes, while dynamic tracking frameworks rely on explicit camera pose estimation or separate motion models. We propose Flow4R, a unified framework that treats camera-space scene flow as the central representation linking 3D structure, object motion, and camera motion. Flow4R predicts a minimal per-pixel property set—3D point position, scene flow, pose weight, and confidence—from two-view inputs using a Vision Transformer. This flow-centric formulation allows local geometry and bidirectional motion to be inferred symmetrically with a shared decoder in a single forward pass, without requiring explicit pose regressors or bundle adjustment. Trained jointly on static and dynamic datasets,

Flow4R achieves state-of-the-art performance on 4D reconstruction and tracking tasks, demonstrating the effectiveness of the flow-central representation for spatiotemporal scene understanding. <https://shenhanqian.github.io/flow4r>

1. Introduction

1.1. A Unified Representation for Dynamic Scenes

Understanding dynamic 3D scenes requires reasoning jointly about *geometry*, *motion*, and *time*. Yet existing methods typically treat these factors separately: multi-view reconstruction systems assume static worlds with fixed camera poses, while motion estimation and tracking frameworks rely on explicit pose regression or per-object motion models. This separation leads to brittle pipelines that struggle to generalize across diverse scenes and motion

types. We argue that a single, unified representation—**scene flow**—can encapsulate both 3D structure and motion, bridging the gap between reconstruction and tracking.

In this work, we introduce **Flow4R**—see Figures 1 and 2—a two-view transformer framework that formulates 4D perception entirely in terms of scene flow. Flow4R predicts per-pixel 3D positions, flow vectors, and camera pose weights, allowing it to infer both camera and object motion in a single forward pass without explicit pose heads or bundle adjustment. Unlike DUS3R-style shared-frame pointmaps, we predict camera-space scene flow with pose weights, enabling motion recovery without a dedicated pose regressor. This flow-centric perspective reframes 4D reconstruction as continuous motion reasoning, unifying static and dynamic scene understanding under one compact formulation.

Recent advances in 3D reconstruction have seen the emergence of multi-view, self-attention-based transformers. DUS3R [54] reconstructs geometry by regressing pointmaps directly from image pairs using a transformer, while VGGT [52] generalizes this idea by handling multiple views jointly through global attention across all input images. Subsequent work extends DUS3R and VGGT to dynamic scenes by fine-tuning them on motion-rich datasets, with some methods incorporating correspondence supervision through optical flow or point tracking [9, 70]. These approaches retain the assumption that all points are predicted in a shared reference frame—a natural choice for static scenes but potentially ambiguous in dynamic scenarios.

1.2. Panta Rhei — Everything Flows¹

Motion is relative: the motion we observe in an image results from both the movements of objects in the scene and the movement of the observer. When estimating relative camera motion from an image pair, we typically assume the scene is static; otherwise, dynamic regions must be masked out. Yet, since the Earth is constantly rotating and orbiting, nothing on Earth is truly static. Declaring certain regions as static is essentially a choice of reference coordinate system—those regions are only static relative to that system. In many cases, the ground serves as a natural reference coordinate frame. However, this choice becomes ambiguous when stepping onto or off a moving escalator. As we approach the escalator, our mind treats the first escalator step as static, but as we leave, it treats the landing as static instead. This illustrates that the selection of a reference coordinate system depends on the task at hand. A more general solution may be to learn to predict camera-space scene flow, which is invariant to the choice of reference frame.

A common challenge in learning scene flow [26, 48,

¹Panta Rhei meaning "everything flows", is an aphorism which describes the doctrine of Heraclitus (520-460 BC).

57, 58] is the scarcity of ground-truth data. Most existing datasets are synthetic [26, 27]: accurate but limited in domain. Can we still learn a good model to predict scene flow when camera parameters and depth maps of static scenes constitute the majority of our data, as in DUS3R [54] and VGGT [52]? Absolutely. Given ground-truth camera intrinsics, the depth of an input view, and its relative pose to another view, we can compute a so-called *rigid flow* to directly supervise the predicted scene flow, since they coincide for static scenes. For dynamic scenes, we can estimate a rigid transformation from the predicted scene flow, using a pose weight map that describes the spatial distribution of reliable static pixels. Combining the predicted rigid transformation with depth yields the predicted rigid flow, which can then be supervised in the same way as for static scenes. The pose weight map is learned by our network in an unsupervised manner to capture common choices of reference coordinate systems in the training datasets. During inference, this map can be replaced to allow flexible switching of the reference coordinate system.

In addition to relativity, motion arises from sequential data. Under our two-view setup, we can take one frame as the anchor, pairing it with subsequent frames to infer the scene structure and relative motion with respect to a consistent reference, the anchor frame. In this way, we can sequentially track 3D points, and solve for the motion of the camera and objects.

In summary, our contributions include:

- A minimal formulation under the two-view setting that supports various 4D tasks.
- An effective supervision strategy to learn local geometry and relative motion in a unified manner.
- A compact and competitive model for 4D reconstruction and tracking.

2. Related Work

2.1. Structure-from-Motion (SfM)

Classical Structure-from-Motion methods [28, 31, 38, 44] typically rely on a modular three-stage pipeline, comprising keypoint extraction & matching, triangulation & registration, and bundle adjustment. These approaches use multi-view geometric constraints to explicitly optimize both the 3D points and camera poses, resulting in accurate and robust reconstructions. Later works [23, 51] make the pipeline fully differentiable, training in an end-to-end manner to make each component more robust. However, they still rely on iterative bundle adjustment optimization, which limits their speed, especially at large scale. Furthermore, they are limited to sparse reconstructions.

The recent work DUS3R [54] opened the way for feed-forward 3D reconstruction using transformer-based architectures. It directly regresses pixel-aligned pointmaps for

two input views in a shared coordinate frame, enabling dense reconstruction without explicit feature matching or optimization. Several follow-up works have been proposed to process more than two views. Spann3R [49] and related methods [5, 53] extend DUS3R to sequential multi-view data, while VGGT [52] and similar approaches [8, 17, 46, 56, 64] process multiple images jointly to estimate consistent geometry. Many methods rely on a dedicated head for camera-pose regression, whereas Flow4R implicitly learns the camera pose via scene flow and pose weight maps. Note that the pose weight map not only excludes dynamic regions but also indicates which static regions are more reliable for camera pose estimation.

2.2. Dynamic Reconstruction and Point Tracking

Compared to 3D reconstruction of static scenes, dynamic reconstruction is considerably more challenging, as traditional multi-view geometric constraints no longer hold for dynamically changing correspondences. The early work DynamicFusion [29] employs a canonical model to represent the dynamic object and tracks non-rigid deformations through a warp field. However, it relies on RGB-D input and is highly sensitive to initialization.

Learning-based methods aim to overcome these limitations by leveraging data-driven priors. Some approaches [6, 18, 21, 69, 71] combine learning with classical optimization to improve robustness and accuracy. For instance, MonST3R [69] fine-tunes DUS3R [54] to regress pointmap pairs for dynamic scenes, and combines them with post-optimization. MegaSAM [21] and BA-Track [6] include predicted motion clues into dense bundle adjustment to achieve stable dynamic reconstruction. Recent methods [9, 11, 41, 70] extend the DUS3R [54] architecture to directly regress dynamic points or point tracks in 3D. Given two views at different timestamps, ZeroMSF [22], Dynamic Point Maps [41], and POMATO [70] add regression heads for pointmaps at different timestamps, while St4RTrack [9] and D²US3R [11] repurpose pointmap heads to predict for the second timestamp. In contrast to these head-bound formulations, Flow4R predicts a compact and flexible set of properties that contain complete geometry and bidirectional motion information with a shared decoder and head.

Concurrent work further extends VGGT [52] to sequential inputs [75], dynamic scenes [12, 73], and 3D point tracking [2, 16, 25, 42, 50, 63, 68], exhibiting high consistency via a single step of feedforward inference. Flow4R focuses on a two-view setting but can be easily enhanced with a similar multi-view attention mechanism.

Another line of work requires depth as the input. DELTA [30] utilizes a dense, efficient architecture to lift 2D pixel-tracks into 3D. By incorporating depth as a core input modality, DELTA maintains high-resolution spatial consistency across long-range sequences. More recently,

TAPIP3D [67] advances this further by introducing a world-centric 3D feature cloud, allowing for persistent tracking even through significant camera ego-motion or temporary occlusions.

3. Method

In this section, we first define a minimal set of properties and show how it can unify 4D reconstruction and tracking tasks in a concise way. Then we describe how this formulation enables a simpler network design and allows flexible processing of sequential data. Please refer to the supplementary material for a summary table of notations.

3.1. A Minimal Property Set for 4D Tasks

Formulation. Given a pair of images $(\mathbf{I}, \mathbf{I}')$ captured from different viewpoints and time stamps, we define for pixels in the image \mathbf{I} with respect to image \mathbf{I}' a minimal property set $\mathcal{S}(\mathbf{I}, \mathbf{I}') = \{\mathbf{P}, \mathbf{F}, \mathbf{W}, \mathbf{C}\}$, where $\mathbf{P} \in \mathbb{R}^{H \times W \times 3}$ is a point position map that places pixels in the local Euclidean space; $\mathbf{F} \in \mathbb{R}^{H \times W \times 3}$ is a scene flow map that moves each point from \mathbf{I} to \mathbf{I}' as a result of camera and object motion; $\mathbf{W} \in (0, 1)^{H \times W}$ is a pose weight map with $\sum_i^{HW} \mathbf{W}^i = 1$, indicating which pixels are more reliable to solve for the camera pose; $\mathbf{C} \in (1, \infty)^{H \times W}$ is a confidence map. The same property set $\mathcal{S}(\mathbf{I}', \mathbf{I}) = \{\mathbf{P}', \mathbf{F}', \mathbf{W}', \mathbf{C}'\}$ can be defined for the image \mathbf{I}' with respect to image \mathbf{I} in a *symmetric* manner. This minimal property set forms a compact parameter space for neural network prediction while allowing flexible combination to serve for varied downstream tasks discussed next.

Scene Flow Decomposition. Induced by both camera and object movements, a scene flow vector \mathbf{F}^i carries a point \mathbf{P}^i to its corresponding location in the other frame's coordinate system and timestamp:

$$\mathbf{P}_{vt}^i = \mathbf{P}^i + \mathbf{F}^i, \quad (1)$$

where i is the pixel index, v and t indicate a switch of view and time from \mathbf{I} to \mathbf{I}' . With the pose weight map \mathbf{W} , we can decompose the camera movement \mathbf{T} by solving the weighted least-squares equation:

$$\hat{\mathbf{T}} = \arg \min_{\mathbf{T} \in SE(3)} \sum_{i=1}^{HW} \mathbf{W}^i \|\mathbf{P}_{vt}^i - \mathbf{T} \mathbf{P}^i\|_2. \quad (2)$$

Thus, each point \mathbf{P}^i in the other view is simply written as

$$\mathbf{P}_v^i = \hat{\mathbf{T}} \mathbf{P}^i. \quad (3)$$

Finally, we can decompose the scene flow vector \mathbf{F}^i into a rigid part (camera motion)

$$\mathbf{F}_v^i = \mathbf{P}_v^i - \mathbf{P}^i, \quad (4)$$

and a non-rigid part (object motion)

$$\mathbf{F}_t^i = \mathbf{F}^i - \mathbf{F}_v^i. \quad (5)$$

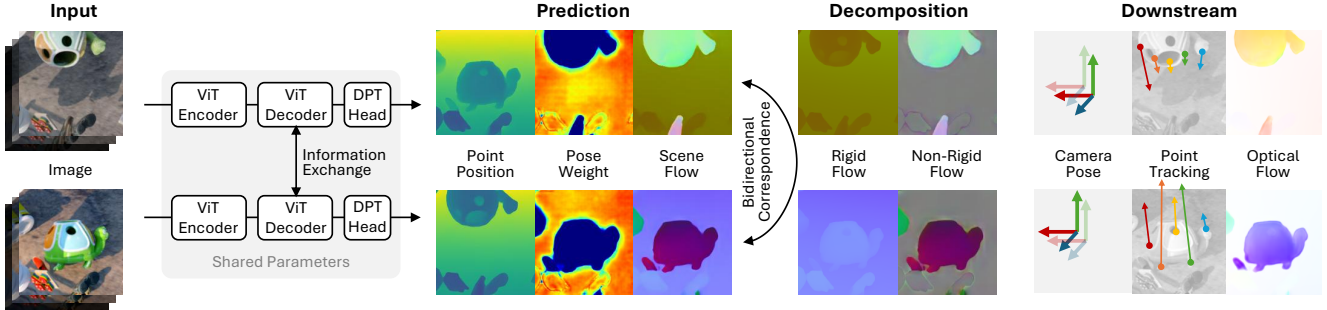


Figure 2. **Flow4R** takes two images as input at a time and predicts a pixel-aligned property set, including point position \mathbf{P} , scene flow \mathbf{F} , pose weight \mathbf{W} , and confidence \mathbf{C} (omitted in this figure), from which various downstream predictions can be deduced.

3D Point Tracking. One can track the location of each point \mathbf{P}^i in its own space with

$$\mathbf{P}_t^i = \hat{\mathbf{T}}^{-1} \mathbf{P}_{vt}^i = \hat{\mathbf{T}}^{-1} (\mathbf{P}^i + \mathbf{F}^i). \quad (6)$$

Focal Length. With the local point map \mathbf{P} , we can solve for the focal length in image \mathbf{I} via

$$\hat{f} = \arg \min_f \sum_i \left(\|\hat{\mathbf{p}}^i - \pi(f, \mathbf{c}, \mathbf{P}^i)\|^2 \right), \quad (7)$$

where $\hat{\mathbf{p}}^i$ and \mathbf{c} are the image coordinates of pixel i and optical center; $\pi(f, \mathbf{c}, \mathbf{P}^i)$ is the projection function which projects a 3D point to the image plane. Here we assume identical focal lengths for both axes.

Optical Flow. Given the estimated or ground-truth focal length f , one can project each \mathbf{P}^i and \mathbf{P}_{vt}^i into the image coordinate space:

$$\mathbf{p}^i = \pi(f, \mathbf{c}, \mathbf{P}^i). \quad (8)$$

In turn, the optical flow can be computed as

$$\mathbf{f}^i = \mathbf{p}_{vt}^i - \mathbf{p}^i. \quad (9)$$

3.2. Flexible Predictions with a Compact Model

As shown above, the minimal property set \mathcal{S} is compact yet sufficient to recover local geometry and relative motion between two images, therefore being an ideal learning target for a vision foundation model.

Architecture Simplicity. As shown by DUST3R [54], a two-view transformer with cross-attention can effectively match two images and reconstruct a scene cohesively. MAST3R [19] extends DUST3R to learn explicit correspondences between images. Therefore, it is natural to use the two-view transformer to learn scene flow between views. Thanks to the symmetry of our formulation, the twin forward paths can share the same parameters for not only the encoders but also the decoders and heads. This also frees us from manually constructing symmetrized pairs during training like DUST3R.

Inference Flexibility. During inference, the predicted property set \mathcal{S} for each image carries both local geometry and relative motion with respect to the other image, supporting not only consistent reconstruction but also bidirectional tracking and coordinate space transformation. In contrast, recent methods either add heads [41, 70] or repurpose an existing head [9, 11] with limited flexibility for timestamp and viewpoint switch.

Sequence Processing. The two-view formulation can be applied to video sequences by constructing image pairs, as shown in Fig. 3. MonST3R [69] constructs pairs within local windows and uses post-optimization to arrange pairs in a pose graph. In contrast, St4Track [9] builds anchored connections to conduct consistent tracking from the first image. To target tracking and reconstruction without post-optimization, we adopt anchored connections following St4Track.

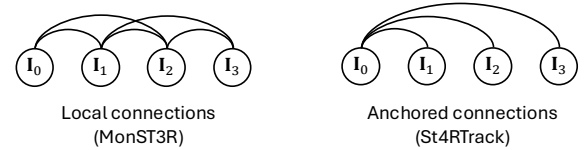


Figure 3. Sequence processing paradigms.

As Flow4R predicts local point maps for both input views, we can align the scale of predictions using the anchor view. Given predictions for anchored pairs $[(\mathbf{I}_0, \mathbf{I}_1), (\mathbf{I}_0, \mathbf{I}_2), (\mathbf{I}_0, \mathbf{I}_3), \dots]$, we compute the average norms s_n of point positions \mathbf{P} for \mathbf{I}_0 in each pair, then align the predicted positions and flows of subsequent pairs by the scaling factors $\frac{s_1}{s_2}, \frac{s_1}{s_3}, \dots$. Note that such scale alignment is not possible for methods that do not predict a local point map for the anchor view [9, 70].

3.3. Model Training

In order to train the network, we pursue supervision signals on the predicted property set \mathcal{S} . In the following, we discuss

supervision regarding the property set $\mathcal{S}(\mathbf{I}, \mathbf{I}')$, while the same supervision applies to its symmetric set $\mathcal{S}(\mathbf{I}', \mathbf{I})$.

Normalization. Following DUST3R [54], we normalize the ground-truth and predicted point maps by their mean Euclidean norms separately for scale-invariance. For simplicity, we assume that all points, including \mathbf{P} , \mathbf{P}_v , and \mathbf{P}_{vt} have been normalized for the rest of this section.

Point Position Loss. With ground-truth point map $\bar{\mathbf{P}}$ obtained by back-projecting the ground-truth depth map with camera intrinsics, we supervise the predicted point map \mathbf{P} in a confidence-weighted way:

$$\mathcal{L}_{\mathbf{P}} = \frac{1}{|\mathbf{M}_{\mathbf{P}}|} \sum_i \mathbf{M}_{\mathbf{P}}^i (\mathbf{C}^i \|\mathbf{P}^i - \bar{\mathbf{P}}^i\|_2 - \alpha \log \mathbf{C}^i), \quad (10)$$

where $\mathbf{M}_{\mathbf{P}}$ indicates pixels with valid depth ground truths.

3D Motion Loss. In our formulation, scene flows play a key role in bridging views and moments. However, ground-truth scene flows are scarcely available, especially for dynamic scenes. Therefore, we consider all types of data that provides pixel-wise correspondences on dynamic objects. This includes scene flow, optical flow, and point tracking. Scene flow and optical flow are dense but only defined between adjacent frames. Point tracking is sparser but carries longer-term correspondences across frames. Fortunately, they can all be converted into camera-space scene flow between two images and utilized to supervise our flow prediction. Meanwhile, we empirically observe better performance when directly predicting and supervising \mathbf{P}_{vt} rather than \mathbf{F} (Tab. 3), although they are interchangeable given $\mathbf{F} = \mathbf{P}_{vt} - \mathbf{P}$. Therefore, let $\mathcal{P} = \{\mathbf{P}, \mathbf{P}_{vt}, \mathbf{W}, \mathbf{C}\}$ be the direct output of each network branch, and adjust the supervisions accordingly.

For ground-truth scene flow and 3D point tracking, we apply the 3D motion loss:

$$\mathcal{L}_{\mathbf{F}} = \frac{1}{|\mathbf{M}_{\mathbf{F}}|} \sum_i \mathbf{M}_{\mathbf{F}}^i (\mathbf{C}^i \|\mathbf{P}_{vt}^i - \bar{\mathbf{P}}_{vt}^i\|_2 - \alpha \log \mathbf{C}^i), \quad (11)$$

where $\mathbf{M}_{\mathbf{F}}^i$ denotes the mask for pixels with ground-truth scene flows or tracked 3D points. Considering that both the scene flow map and point position map are defined in the Euclidean space, we share the confidence map between them for simplicity. Besides, the confidence score gradually grows as training proceeds, implicitly up-weighting the scene flow loss along with the point position loss.

2D Motion Loss. When ground-truth optical flow or 2D point tracking are available, we apply the 2D motion loss to \mathbf{p}_{vt} (Eq. (9)):

$$\mathcal{L}_{\mathbf{f}} = \frac{1}{|\mathbf{M}_{\mathbf{f}}|} \sum_i \mathbf{M}_{\mathbf{f}}^i \|\mathbf{p}_{vt}^i - \bar{\mathbf{p}}_{vt}^i\|_2. \quad (12)$$

We don't use confidence weighting here because \mathbf{p}_{vt} lies in the 2D projective space rather than the Euclidean space.

Pose Weight Loss. Considering that the scene flow contains all the motion information, we only need to know where to look at when solving for the camera pose, which is why we need a pose weight map \mathbf{W} . However, it is not straightforward to obtain ground truths for it. Although foreground masks, instance masks, and rigidity masks are available for some datasets, they are not identical to what the pose weight map is supposed to be. Specifically, foreground objects can still be useful for localization when they are not moving, and the rigidity score can be ambiguous for an object moving at an infinitesimally low speed. Indeed, the pose weight map \mathbf{W} can be useful not only for filtering out non-static regions in a dynamic scene but also for down-weighting unreliable pixels in regions that are far away, reflective, or occluded.

Therefore, we seek to learn the pose weight map in a self-supervised way:

$$\mathcal{L}_{\mathbf{W}} = \frac{1}{|\mathbf{M}_{\mathbf{P}}|} \sum_i \mathbf{M}_{\mathbf{P}}^i (\|\mathbf{P}_v^i - \bar{\mathbf{P}}_v^i\|_2). \quad (13)$$

$\mathbf{P}_v^i = \hat{\mathbf{T}} \mathbf{P}^i$ where $\hat{\mathbf{T}}$ is the camera pose solved from \mathbf{P} , \mathbf{P}_{vt} , and \mathbf{W} (Eqs. (2) and (3)). $\bar{\mathbf{P}}_v^i = \bar{\mathbf{T}} \bar{\mathbf{P}}^i$, where $\bar{\mathbf{T}}$ is the ground-truth camera pose of \mathbf{I} relative to \mathbf{I}' . When computing \mathbf{P}_v , we stop gradients for \mathbf{P} and \mathbf{P}_{vt} since they are sufficiently supervised in other loss terms. Thereby, \mathbf{W} becomes the only property that receives gradients. Intuitively, this loss term adjusts \mathbf{W} so that the solved camera pose aligns with the ground truth.

Rigid Motion Loss. Given the scarcity of scene flow (point tracking) annotations, augmenting motion supervision with the rigid motion induced by ground-truth camera pose is a natural choice. This leads to the rigid motion loss

$$\mathcal{L}_{\mathbf{F}_v} = \frac{1}{|\mathbf{M}_{\mathbf{P}}|} \sum_i \mathbf{M}_{\mathbf{P}}^i (w^i \mathbf{C}^i \|\mathbf{P}_{vt}^i - \bar{\mathbf{P}}_v^i\|_2 - \alpha \log \mathbf{C}^i), \quad (14)$$

where

$$w^i = \begin{cases} sg(\mathbf{W}^i) \times HW & \text{if dynamic dataset,} \\ 1 & \text{if static dataset.} \end{cases} \quad (15)$$

For dynamic scenes, the predicted pose weight map \mathbf{W}^i is multiplied to down-weight the loss for non-static regions. Since $\sum_i^{HW} \mathbf{W}^i = 1$, we scale \mathbf{W}^i up by HW for a comparable loss scale as others. $sg(\cdot)$ stops gradient backpropagation so that \mathbf{W} is not optimized by this term. For static scenes, \mathbf{P}_{vt} is equivalent to \mathbf{P}_v , thus can be regressed to $\bar{\mathbf{P}}_v^i$ with w^i set to one.

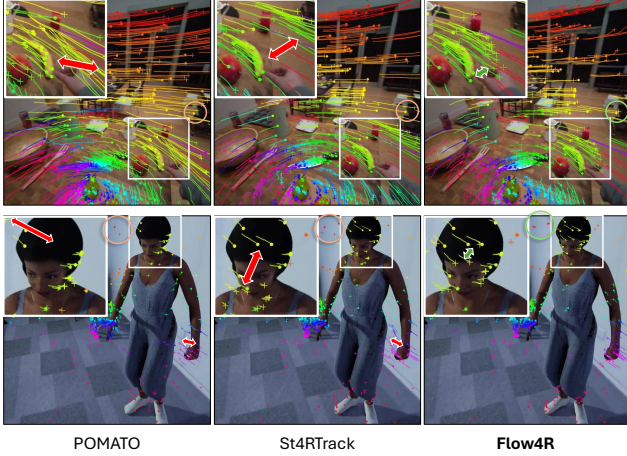


Figure 4. **Qualitative Results.** We visualize the 3D tracking trajectories by projecting them onto 2D. Ground-truth trajectories are marked with dots (\bullet), and predicted trajectories are denoted by a plus symbol ($+$). The results of Flow4R show less reprojection error on both the background and foreground.

Total Loss. The total loss function is written as

$$\mathcal{L}(\mathbf{P}, \mathbf{P}_{vt}, \mathbf{W}, \mathbf{C}) = \lambda_1 \mathcal{L}_{\mathbf{P}} + \lambda_2 \mathcal{L}_{\mathbf{F}} + \lambda_3 \mathcal{L}_{\mathbf{f}} \quad (16)$$

$$+ \lambda_4 \mathcal{L}_{\mathbf{W}} + \lambda_5 \mathcal{L}_{\mathbf{F}_v} \quad (17)$$

with $\lambda_1 = 1$, $\lambda_2 = \lambda_4 = \lambda_5 = 0.5$, $\lambda_3 = 0.3$, and $\alpha = 0.2$ in Eqs. (10), (11) and (14).

4. Experiments

Training Details. The training data is a combination of static and dynamic, real-world and synthetic datasets, including Habitat [34, 37, 45], Blended-MVS [65], MegaDepth [20], ARKitScenes [3], CO3D [35], Static Scenes 3D [39], ScanNet++ [66], Waymo [43], TartanAir [55], UnReal4K [47], WildRGBD [61], DL3DV [24], MapFree [1], ScanNet [7], HyperSim [36], Virtual KITTI 2 [4], Spring [27], PointOdyssey [72], Dynamic Replica [14], Kubric [10], and OmniWorld-Game [74]. For some datasets, we use the data processing code or preprocessed data by DUSt3R [54], CUT3R [53], MonST3R [69], and CoTracker [15]. Among the dynamic datasets, Virtual KITTI 2 provides ground-truth scene flow; Spring, Dynamic Replica, and OmniWorld-Game have ground-truth optical flow; PointOdyssey, Dynamic Replica, and Kubric contain 3D point tracking annotations.

Unlike most of our baselines that are finetuned from DUSt3R [54], MASt3R [19], or MonST3R [69], we initialize Flow4R from CroCo [59, 60] due to the formulation change and train it in two stages. In the first stage, we train the model with a linear head for 100 epochs on images at resolution 224. We sample 900K pairs for each epoch. In the second stage, we train the model with a DPT head for

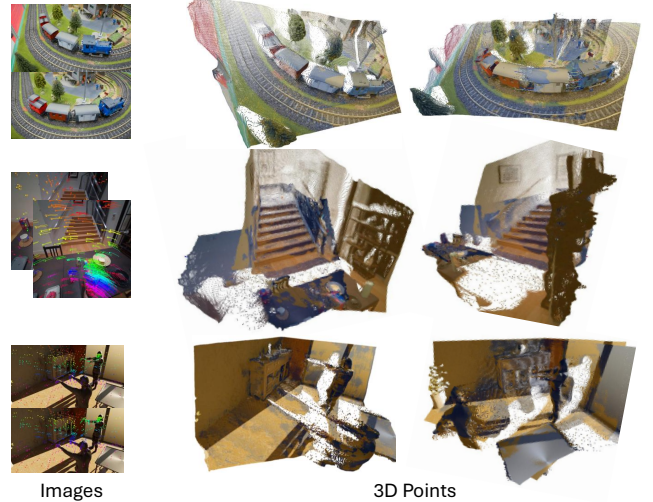


Figure 5. **3D Visualization of the Predictions.** Examples are taken from the DAVIS [33], Aria Digital Twin [32], and Point Odyssey [72] datasets. Our model is capable of reconstructing 3D scenes and tracking the motion of both the camera and objects.

100 epochs on images at resolution 512 with random aspect ratios. We sample 84K pairs for each epoch in the second stage. For video datasets, we first sample a random frame and then pair it with a neighbor within 50 frames of the same scene. We use the Adam optimizer with linear learning rate warmup (10 epochs for the first stage, 20 epochs for the second stage) to reach the peak learning rate 1e-4, then decay to 1e-6 until the end following a cosine curve. Gradients are clipped to a maximum norm of 10 with directions preserved. We use a total batch size of 256 across eight NVIDIA A100/H100 GPUs for resolution 224 and batch size 64 for resolution 512. The entire training process takes around four days in total.

4.1. Tracking and Reconstruction

Benchmarks and Metrics. Since we focus on reconstruction and tracking in a consistent coordinate system, we follow St4RTrack [9] to conduct evaluation in world coordinates using the WorldTrack [9] benchmark. For 3D point tracking, WorldTrack comprises two real-world datasets, Aria Digital Twin [32] and Panoptic Studio [13], as well as two synthetic datasets from the test sets of Point Odyssey [72] and Dynamic Replica [14], which provide 3D point trajectories. For dynamic 3D reconstruction, the synthetic Point Odyssey dataset and the real-world TUM-Dynamics [40] dataset are used for testing.

Following St4RTrack [9], we adopt the Average Percentage of 3D Points within Delta (APD3D) metric for 3D point tracking evaluation. The predicted 3D point trajectories, after alignment to the ground truth, are compared frame by frame. We compute the prediction error and report the

Table 1. World Coordinate 3D Point Tracking. We report the performance on four datasets, Aria Digital Twin (ADT), Dynamic Replica (DR), and Point Odyssey (PO), and Panoptic Studio (PS) using the Average Points under Distance (APD3D \uparrow) metric for all points and dynamic points after global median alignment. We also compare the model sizes in the last column. The best and second-best results are marked in bold and underlined.

	All Points				Dynamic Points			# param. (B)
	ADT	DR	PO	PS	ADT	DR	PO	
MonST3R	74.4	58.1	33.5	51.3	67.9	51.9	39.4	0.7
SpaTracker	45.7	54.9	38.5	62.6	67.7	58.7	51.2	0.2
POMATO	57.2	68.4	49.7	64.9	78.1	62.7	58.1	0.7
St4RTrack	76.0	73.7	68.0	69.7	75.3	68.1	68.7	0.7
Flow4R	78.6	78.5	71.1	64.3	70.9	77.2	72.9	<u>0.4</u>

percentage of points whose error falls below a threshold $\delta_{3D} \in \{0.1m, 0.3m, 0.5m, 1.0m\}$, averaged over the first 64 frames. For dynamic 3D reconstruction, we compare reconstructed point clouds against the ground truth using both APD3D and End-Point Error (EPE) metrics.

Baselines. Flow4R is primarily compared with other feedforward tracking and reconstruction methods. For 3D point tracking, we evaluate against a camera-coordinate 3D tracking method, SpatialTracker [62], a dynamic 3D reconstruction method, MonST3R [69], and two dynamic 3D tracking methods POMATO [70] and St4RTrack [9]. For POMATO, since its sequential model only provides tracking from other frames to the anchor frame (rather than the standard anchor-to-other-frame tracking used by other methods), we adopt its pairwise model for evaluation. For 3D reconstruction evaluation, the static methods DUS3R [54] and MAS3R [19] are also compared.

Results. In Tab. 1, we conduct evaluation on world coordinate 3D point tracking, which is essentially \mathbf{P}_t (Eq. (6)) for Flow4R. As the APD metric measures how accurate points are tracked in world space, a model needs to predict high-quality geometry, camera motion, and point movement at the same time. Flow4R shows higher performance on most datasets despite having fewer parameters. Note that all the baselines except SpaTracker follow the asymmetric head-bound formulation of DUS3R, while Flow4R’s competence indicates the potential of our symmetric minimal formulation.

In Tab. 2, we evaluate the world-space reconstruction quality via point maps in the reference view, which corresponds to \mathbf{P}_v (Eq. (3)) in our formulation. Flow4R outperforms most baselines including those relying on post-optimization. This further validates the capacity and potential of our formulation with reconstruction and tracking unified by scene flows.

As a qualitative comparison, we show sample results of

Table 2. World Coordinate 3D Reconstruction. We report performance on Point Odyssey and TUM-Dynamics after global median scaling. The best and second-best results are marked in bold and underlined.

Category	Method	Point Odyssey		TUM-Dynamics	
		APD \uparrow	EPE \downarrow	APD \uparrow	EPE \downarrow
w/ Global Align.	DUS3R+GA	43.90	0.609	70.49	0.315
	MAS3R+GA	60.44	0.403	68.38	0.519
	MonST3R+GA	72.31	0.263	63.87	0.343
Feedforward	DUS3R	45.79	0.639	72.26	0.289
	MAS3R	56.90	0.464	66.22	0.551
	MonST3R	68.25	0.304	61.38	0.365
	POMATO	66.50	0.385	49.80	0.509
	St4RTrack	<u>78.73</u>	<u>0.205</u>	83.42	0.185
	Flow4R	81.00	0.182	79.87	0.202

the most competitive baselines in Fig. 4. Flow4R predicts point positions precisely and tracks the motion of moving parts effectively.

4.2. Ablation Study

Based on the minimal property set \mathcal{S} defined in Sec. 3.1, it is intuitive to have the network directly predict the scene flow \mathbf{F} . However, as reconstruction and tracking accuracy are the primary objectives for real-world applications, we ablate three variants of Flow4R. Specifically, the network can predict either \mathbf{F} or \mathbf{P}_{vt} and derive the alternative via Eq. (1). Furthermore, the regression target can be either $\bar{\mathbf{F}}$ or $\bar{\mathbf{P}}_{vt}$. Interestingly, we find that directly predicting \mathbf{P}_{vt} while supervising with $\bar{\mathbf{P}}_{vt}$ yields superior performance (Tab. 3). This may be because \mathbf{P}_{vt} is more directly related to the final evaluation metrics, which are based on point positions. In contrast, \mathbf{F} is an intermediate representation that requires additional transformations to compute the final point positions, potentially introducing more sources of error.

Table 3. Ablation Study on Motion Representation. We compare three variants of Flow4R using the Average Points under Distance (APD3D \uparrow) metric across all points. Our results demonstrate that directly predicting \mathbf{P}_{vt} and supervising it with its corresponding ground truth yields the optimal performance across all datasets. For efficiency, these ablation results are reported from models trained for half the total number of epochs, which is sufficient to observe relative performance trends.

Pred.	Target	Tracking				Reconstruction	
		ADT	DR	PO	PS	PO	TUM
\mathbf{F}	$\bar{\mathbf{F}}$	78.03	73.26	60.23	55.80	<u>69.36</u>	79.78
\mathbf{F}	\mathbf{P}_{vt}	77.72	<u>76.41</u>	<u>61.21</u>	<u>63.69</u>	66.29	80.05
\mathbf{P}_{vt}	$\bar{\mathbf{P}}_{vt}$	78.50	78.48	67.93	67.17	77.20	80.34

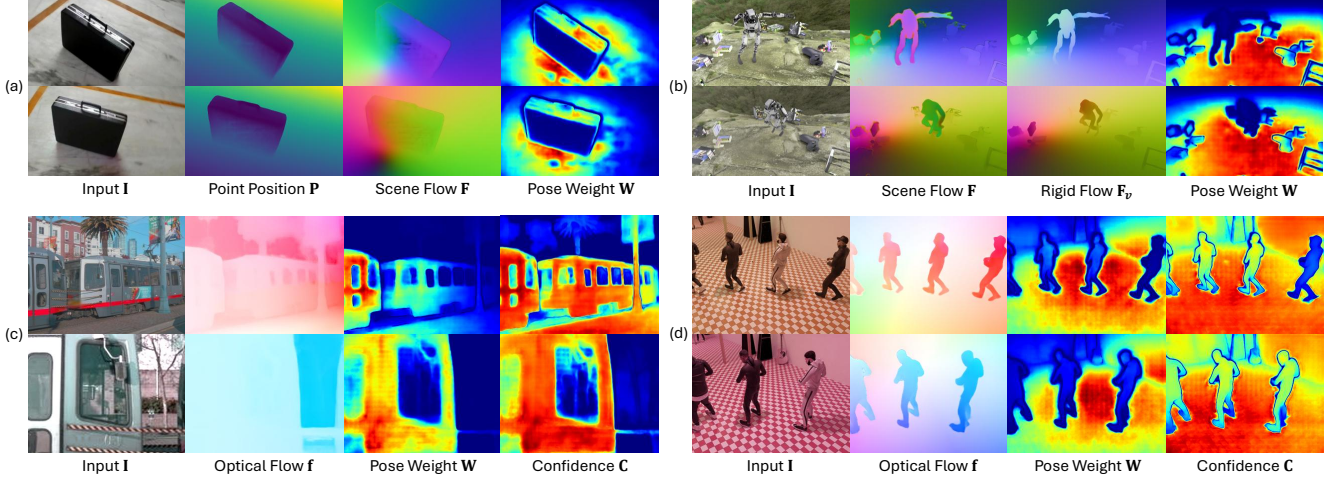


Figure 6. **2D Visualizations of Flow4R Predictions (Sec. 4.3).** Given an image pair, Flow4R predicts for each image the point position \mathbf{P} , scene flow \mathbf{F} , pose weight \mathbf{W} , and confidence \mathbf{C} . The point position map \mathbf{P} captures scene geometry in the local space. The scene flow map \mathbf{F} describes how each point moves from the current image to its pair, capturing both camera and object motions. The pose weight map \mathbf{W} indicates which pixels are reliable for camera pose estimation. The confidence map \mathbf{C} indicates the uncertainty of the predictions.

4.3. Visualizations

To illustrate the internal of Flow4R, we visualize its predictions across diverse scenarios. In Fig. 6 (a), a static scene featuring a suitcase is shown. The predicted scene flow map exhibits varied colors across all directions, indicating that camera motion is dominated by rotation. Conversely, the pose weight map assigns low values to the dark, textureless regions of the suitcase, as these areas provide minimal utility for localization. Fig. 6 (b) captures a dynamic environment where objects surround a jumping robot. Here, the scene flow map aligns with the rigid flow map, except in the region of the moving robot. Consequently, the pose weight map strongly suppresses the robot’s pixels to prevent its independent motion from biasing the camera pose estimation. In Fig. 6 (c), which depicts a stopped train from both far and near perspectives, the optical flow maps—derived from point positions and scene flow—are dominated by red and blue hues. This pattern signifies a primarily translational camera motion. Notably, the pose weight map isolates the overlapping regions between the two photographs; this significantly enhances the interpretability of our camera pose estimation by explicitly identifying the pixels used for the calculation. Finally, Fig. 6 (d) records four individuals dancing in a room. The confidence map reveals high certainty across the scene, except for the last person in the line, who appears in only one image. Simultaneously, the pose weight map excludes all moving figures, ensuring the camera pose is estimated solely from the static background.

In Fig. 5, we render the reconstructed and tracked points within a global coordinate system. Both dynamic elements (such as the train and human figures) and stationary structures (including the tree, ladder, wall, and table) exhibit

high 3D consistency, demonstrating the effectiveness of our flow-centric tracking and reconstruction pipeline.

5. Conclusion

We introduced **Flow4R**, a unified framework for 4D reconstruction and tracking that treats *flow as the central representation* of geometry and motion. By learning a minimal property set (3D point positions, scene flow, pose weight, and confidence), Flow4R achieves consistent 4D reasoning across static and dynamic scenes without separate pose regressors or bundle adjustment. Our two-view transformer, trained on static and dynamic datasets, disentangles rigid and non-rigid motion and scales to long video sequences via anchored pairs. We believe this formulation opens a promising path toward holistic 4D perception—where reconstruction, tracking, and scene understanding emerge from one coherent flow field rather than a collection of separate tasks.

Flow4R unifies reconstruction and tracking with a compact two-view formulation and matches DUST3R-style methods with similar data. However, the limited availability of scene flow data still constrains flow quality relative to depth. Our study focuses on two-view inputs; multi-view setups like VGGT [52] could further leverage attention capacity. Online tracking under tight memory and compute remains an open question.

Acknowledgments

This work was supported by the ERC Advanced Grant “SIMULACRON” (agreement #884679), the GNI Project “AI4Twinning”, the DFG project CR 250/26-1 “4DY-outube”, and the UKRI AIRR programme.

References

[1] Eduardo Arnold, Jamie Wynn, Sara Vicente, Guillermo Garcia-Hernando, Aron Monszpart, Victor Prisacariu, Daniyar Turmukhambetov, and Eric Brachmann. Map-free visual relocalization: Metric pose relative to a single image. In *European Conference on Computer Vision*, pages 690–708. Springer, 2022. [6](#)

[2] Abhishek Badki, Hang Su, Bowen Wen, and Orazio Gallo. L4P: Towards unified low-level 4D vision perception. In *International Conference on 3D Vision (3DV)*, 2026. [3](#)

[3] Gilad Baruch, Zhuoyuan Chen, Afshin Dehghan, Yuri Feigin, Peter Fu, Thomas Gebauer, Daniel Kurz, Tal Dimry, Brandon Joffe, Arik Schwartz, et al. Arkitscenes: A diverse real-world dataset for 3d indoor scene understanding using mobile rgb-d data. In *Thirty-fifth Conference on Neural Information Processing Systems Datasets and Benchmarks Track (Round 1)*. [6](#)

[4] Yohann Cabon, Naila Murray, and Martin Humenberger. Virtual kitti 2. *arXiv preprint arXiv:2001.10773*, 2020. [6](#)

[5] Yohann Cabon, Lucas Stoffl, Leonid Antsfeld, Gabriela Csurka, Boris Chidlovskii, Jerome Revaud, and Vincent Leroy. MUS3R: Multi-view network for stereo 3D reconstruction. In *CVPR*, pages 1050–1060, 2025. [3](#)

[6] Weirong Chen, Ganlin Zhang, Felix Wimbauer, Rui Wang, Nikita Araslanov, Andrea Vedaldi, and Daniel Cremers. Back on track: Bundle adjustment for dynamic scene reconstruction. In *Proceedings of the IEEE/CVF International Conference on Computer Vision (ICCV)*, pages 4951–4960, 2025. [3](#)

[7] Angela Dai, Angel X Chang, Manolis Savva, Maciej Halber, Thomas Funkhouser, and Matthias Nießner. Scannet: Richly-annotated 3d reconstructions of indoor scenes. In *Proceedings of the IEEE conference on computer vision and pattern recognition*, pages 5828–5839, 2017. [6](#)

[8] Sven Elflein, Qunjie Zhou, and Laura Leal-Taixé. Light3r-sfm: Towards feed-forward structure-from-motion. In *Proceedings of the Computer Vision and Pattern Recognition Conference*, pages 16774–16784, 2025. [3](#)

[9] Haiwen Feng*, Junyi Zhang*, Qianqian Wang, Yufei Ye, Pengcheng Yu, Michael J. Black, Trevor Darrell, and Angjoo Kanazawa. St4RTrack: Simultaneous 4D reconstruction and tracking in the world. In *Proceedings of the IEEE/CVF International Conference on Computer Vision*, 2025. [2](#), [3](#), [4](#), [6](#), [7](#)

[10] Klaus Greff, Francois Belletti, Lucas Beyer, Carl Doersch, Yilun Du, Daniel Duckworth, David J Fleet, Dan Gnanaprasam, Florian Golemo, Charles Herrmann, et al. Kubric: A scalable dataset generator. In *Proceedings of the IEEE/CVF conference on computer vision and pattern recognition*, pages 3749–3761, 2022. [6](#)

[11] Jisang Han, Honggyu An, Jaewoo Jung, Takuya Narihira, Junyoung Seo, Kazumi Fukuda, Chaehyun Kim, Sunghwan Hong, Yuki Mitsufuji, and Seungryong Kim. Enhancing 3d reconstruction for dynamic scenes. In *The Thirty-ninth Annual Conference on Neural Information Processing Systems*, 2025. [3](#), [4](#)

[12] Yu Hu, Chong Cheng, Sicheng Yu, Xiaoyang Guo, and Hao Wang. Vggt4d: Mining motion cues in visual geometry transformers for 4d scene reconstruction. *arXiv preprint arXiv:2511.19971*, 2025. [3](#)

[13] Hanbyul Joo, Hao Liu, Lei Tan, Lin Gui, Bart Nabbe, Iain Matthews, Takeo Kanade, Shohei Nobuhara, and Yaser Sheikh. Panoptic studio: A massively multiview system for social motion capture. In *Proceedings of the IEEE international conference on computer vision*, pages 3334–3342, 2015. [6](#)

[14] Nikita Karaev, Ignacio Rocco, Benjamin Graham, Natalia Neverova, Andrea Vedaldi, and Christian Rupprecht. Dynamicstereo: Consistent dynamic depth from stereo videos. In *Proceedings of the IEEE/CVF Conference on Computer Vision and Pattern Recognition*, pages 13229–13239, 2023. [6](#)

[15] Nikita Karaev, Ignacio Rocco, Benjamin Graham, Natalia Neverova, Andrea Vedaldi, and Christian Rupprecht. Co-tracker: It is better to track together. In *European conference on computer vision*, pages 18–35. Springer, 2024. [6](#)

[16] Jay Karhade, Nikhil Keetha, Yuchen Zhang, Tanisha Gupta, Akash Sharma, Sebastian Scherer, and Deva Ramanan. Any4d: Unified feed-forward metric 4d reconstruction. *arXiv preprint arXiv:2512.10935*, 2025. [3](#)

[17] Nikhil Keetha, Norman Müller, Johannes Schönberger, Lorenzo Porzi, Yuchen Zhang, Tobias Fischer, Arno Knapsch, Duncan Zauss, Ethan Weber, Nelson Antunes, Jonathon Luiten, Manuel Lopez-Antequera, Samuel Rota Bulò, Christian Richardt, Deva Ramanan, Sebastian Scherer, and Peter Kotschieder. MapAnything: Universal feed-forward metric 3D reconstruction. In *International Conference on 3D Vision (3DV)*. IEEE, 2026. [3](#)

[18] Johannes Kopf, Xuejian Rong, and Jia-Bin Huang. Robust consistent video depth estimation. In *Proceedings of the IEEE/CVF Conference on Computer Vision and Pattern Recognition*, pages 1611–1621, 2021. [3](#)

[19] Vincent Leroy, Yohann Cabon, and Jérôme Revaud. Grounding image matching in 3D with MAST3R. In *European Conference on Computer Vision*, pages 71–91. Springer, 2024. [4](#), [6](#), [7](#)

[20] Zhengqi Li and Noah Snavely. Megadepth: Learning single-view depth prediction from internet photos. In *Proceedings of the IEEE conference on computer vision and pattern recognition*, pages 2041–2050, 2018. [6](#)

[21] Zhengqi Li, Richard Tucker, Forrester Cole, Qianqian Wang, Linyi Jin, Vickie Ye, Angjoo Kanazawa, Aleksander Holynski, and Noah Snavely. Megasam: Accurate, fast and robust structure and motion from casual dynamic videos. In *Proceedings of the Computer Vision and Pattern Recognition Conference*, pages 10486–10496, 2025. [3](#)

[22] Yiqing Liang, Abhishek Badki, Hang Su, James Tompkin, and Orazio Gallo. Zero-shot monocular scene flow estimation in the wild. In *Proceedings of the Computer Vision and Pattern Recognition Conference*, pages 21031–21044, 2025. [3](#)

[23] Philipp Lindenberger, Paul-Edouard Sarlin, Viktor Larsson, and Marc Pollefeys. Pixel-perfect structure-from-motion with featuremetric refinement. In *Proceedings of*

the IEEE/CVF international conference on computer vision, pages 5987–5997, 2021. 2

[24] Lu Ling, Yichen Sheng, Zhi Tu, Wentian Zhao, Cheng Xin, Kun Wan, Lantao Yu, Qianyu Guo, Zixun Yu, Yawen Lu, et al. Dl3dv-10k: A large-scale scene dataset for deep learning-based 3d vision. In *Proceedings of the IEEE/CVF Conference on Computer Vision and Pattern Recognition*, pages 22160–22169, 2024. 6

[25] Xinhang Liu, Yuxi Xiao, Donny Y Chen, Jiashi Feng, Yu-Wing Tai, Chi-Keung Tang, and Bingyi Kang. Trace anything: Representing any video in 4d via trajectory fields. *arXiv preprint arXiv:2510.13802*, 2025. 3

[26] Nikolaus Mayer, Eddy Ilg, Philip Hausser, Philipp Fischer, Daniel Cremers, Alexey Dosovitskiy, and Thomas Brox. A large dataset to train convolutional networks for disparity, optical flow, and scene flow estimation. In *Proceedings of the IEEE conference on computer vision and pattern recognition*, pages 4040–4048, 2016. 2

[27] Lukas Mehl, Jenny Schmalfuss, Azin Jahedi, Yaroslava Nalivayko, and Andrés Bruhn. Spring: A high-resolution high-detail dataset and benchmark for scene flow, optical flow and stereo. In *Proceedings of the IEEE/CVF Conference on Computer Vision and Pattern Recognition*, pages 4981–4991, 2023. 2, 6

[28] Pierre Moulon, Pascal Monasse, Romuald Perrot, and Renaud Marlet. Openmvg: Open multiple view geometry. In *International Workshop on Reproducible Research in Pattern Recognition*, pages 60–74. Springer, 2016. 2

[29] Richard A. Newcombe, Dieter Fox, and Steven M. Seitz. Dynamicfusion: Reconstruction and tracking of non-rigid scenes in real-time. In *The IEEE Conference on Computer Vision and Pattern Recognition (CVPR)*, 2015. 3

[30] Tuan Duc Ngo, Peiye Zhuang, Evangelos Kalogerakis, Chuang Gan, Sergey Tulyakov, Hsin-Ying Lee, and Chaoyang Wang. Delta: Dense efficient long-range 3d tracking for any video. In *The Thirteenth International Conference on Learning Representations*, 2025. 3

[31] Linfei Pan, Dániel Baráth, Marc Pollefeys, and Johannes L Schönberger. Global structure-from-motion revisited. In *ECCV*, pages 58–77. Springer, 2024. 2

[32] Xiaqing Pan, Nicholas Charron, Yongqian Yang, Scott Peters, Thomas Whelan, Chen Kong, Omkar Parkhi, Richard Newcombe, and Yuheng Carl Ren. Aria digital twin: A new benchmark dataset for egocentric 3d machine perception. In *Proceedings of the IEEE/CVF International Conference on Computer Vision*, pages 20133–20143, 2023. 6

[33] Federico Perazzi, Jordi Pont-Tuset, Brian McWilliams, Luc Van Gool, Markus Gross, and Alexander Sorkine-Hornung. A benchmark dataset and evaluation methodology for video object segmentation. In *Proceedings of the IEEE conference on computer vision and pattern recognition*, pages 724–732, 2016. 6

[34] Xavi Puig, Eric Undersander, Andrew Szot, Mikael Dallaire Cote, Ruslan Partsey, Jimmy Yang, Ruta Desai, Alexander William Clegg, Michal Hlavac, Tiffany Min, Theo Gervet, Vladimir Vondrus, Vincent-Pierre Berges, John Turner, Oleksandr Maksymets, Zsolt Kira, Mrinal Kalakrishnan, Jitendra Malik, Devendra Singh Chaplot, Unnat Jain, Dhruv Batra, Akshara Rai, and Rozbeh Mottaghi. Habitat 3.0: A co-habitat for humans, avatars and robots, 2023. 6

[35] Jeremy Reizenstein, Roman Shapovalov, Philipp Henzler, Luca Sbordone, Patrick Labatut, and David Novotny. Common objects in 3d: Large-scale learning and evaluation of real-life 3d category reconstruction. In *Proceedings of the IEEE/CVF international conference on computer vision*, pages 10901–10911, 2021. 6

[36] Mike Roberts, Jason Ramapuram, Anurag Ranjan, Atulit Kumar, Miguel Angel Bautista, Nathan Paczan, Russ Webb, and Joshua M Susskind. Hypersim: A photorealistic synthetic dataset for holistic indoor scene understanding. In *Proceedings of the IEEE/CVF international conference on computer vision*, pages 10912–10922, 2021. 6

[37] Manolis Savva, Abhishek Kadian, Oleksandr Maksymets, Yili Zhao, Erik Wijmans, Bhavana Jain, Julian Straub, Jia Liu, Vladlen Koltun, Jitendra Malik, Devi Parikh, and Dhruv Batra. Habitat: A Platform for Embodied AI Research. In *Proceedings of the IEEE/CVF International Conference on Computer Vision (ICCV)*, 2019. 6

[38] Johannes L Schonberger and Jan-Michael Frahm. Structure-from-motion revisited. In *Proceedings of the IEEE conference on computer vision and pattern recognition*, pages 4104–4113, 2016. 2

[39] Philipp Schröppel, Jan Bechtold, Artemij Amiranashvili, and Thomas Brox. A benchmark and a baseline for robust multi-view depth estimation. In *2022 International Conference on 3D Vision (3DV)*, pages 637–645. IEEE, 2022. 6

[40] Jürgen Sturm, Nikolas Engelhard, Felix Endres, Wolfram Burgard, and Daniel Cremers. A benchmark for the evaluation of rgbd slam systems. In *2012 IEEE/RSJ international conference on intelligent robots and systems*, pages 573–580. IEEE, 2012. 6

[41] Edgar Sucar, Zihang Lai, Eldar Insafutdinov, and Andrea Vedaldi. Dynamic point maps: A versatile representation for dynamic 3d reconstruction. In *Proceedings of the IEEE/CVF International Conference on Computer Vision (ICCV)*, 2025. 3, 4

[42] Edgar Sucar, Eldar Insafutdinov, Zihang Lai, and Andrea Vedaldi. V-dpm: 4d video reconstruction with dynamic point maps. *arXiv preprint arXiv:2601.09499*, 2026. 3

[43] Pei Sun, Henrik Kretzschmar, Xerxes Dotiwalla, Aurelien Chouard, Vijaysai Patnaik, Paul Tsui, James Guo, Yin Zhou, Yuning Chai, Benjamin Caine, et al. Scalability in perception for autonomous driving: Waymo open dataset. In *Proceedings of the IEEE/CVF conference on computer vision and pattern recognition*, pages 2446–2454, 2020. 6

[44] Christopher Sweeney, Tobias Hollerer, and Matthew Turk. Theia: A fast and scalable structure-from-motion library. In *ACM MM*, pages 693–696, 2015. 2

[45] Andrew Szot, Alex Clegg, Eric Undersander, Erik Wijmans, Yili Zhao, John Turner, Noah Maestre, Mustafa Mukadam, Devendra Chaplot, Oleksandr Maksymets, Aaron Gokaslan, Vladimir Vondrus, Sameer Dharur, Franziska Meier, Wojciech Galuba, Angel Chang, Zsolt Kira, Vladlen Koltun, Jitendra Malik, Manolis Savva, and Dhruv Batra. Habitat 2.0: Training home assistants to rearrange their habitat. In *Ad-*

vances in Neural Information Processing Systems (NeurIPS), 2021. 6

[46] Zhenggang Tang, Yuchen Fan, Dilin Wang, Hongyu Xu, Rakesh Ranjan, Alexander Schwing, and Zhicheng Yan. Mv-dust3r+: Single-stage scene reconstruction from sparse views in 2 seconds. In *Proceedings of the Computer Vision and Pattern Recognition Conference*, pages 5283–5293, 2025. 3

[47] Fabio Tosi, Yiyi Liao, Carolin Schmitt, and Andreas Geiger. Smd-nets: Stereo mixture density networks. In *Proceedings of the IEEE/CVF conference on computer vision and pattern recognition*, pages 8942–8952, 2021. 6

[48] Christoph Vogel, Konrad Schindler, and Stefan Roth. Piecewise rigid scene flow. In *Proceedings of the IEEE International Conference on Computer Vision*, pages 1377–1384, 2013. 2

[49] Hengyi Wang and Lourdes Agapito. 3D reconstruction with spatial memory. In *3DV*, 2025. 3

[50] Haonan Wang, Hanyu Zhou, Haoyue Liu, and Luxin Yan. 4d-vggt: A general foundation model with spatiotemporal awareness for dynamic scene geometry estimation. *arXiv preprint arXiv:2511.18416*, 2025. 3

[51] Jianyuan Wang, Nikita Karaev, Christian Rupprecht, and David Novotny. Vggsfm: Visual geometry grounded deep structure from motion. In *Proceedings of the IEEE/CVF conference on computer vision and pattern recognition*, pages 21686–21697, 2024. 2

[52] Jianyuan Wang, Minghao Chen, Nikita Karaev, Andrea Vedaldi, Christian Rupprecht, and David Novotny. Vggt: Visual geometry grounded transformer. In *Proceedings of the Computer Vision and Pattern Recognition Conference*, pages 5294–5306, 2025. 2, 3, 8

[53] Qianqian Wang, Yifei Zhang, Aleksander Holynski, Alexei A Efros, and Angjoo Kanazawa. Continuous 3D perception model with persistent state. In *CVPR*, pages 10510–10522, 2025. 3, 6

[54] Shuzhe Wang, Vincent Leroy, Yohann Cabon, Boris Chidlovskii, and Jérôme Revaud. DUST3R: Geometric 3D vision made easy. 2024 ieee. In *CVF Conference on Computer Vision and Pattern Recognition (CVPR)*, pages 20697–20709, 2023. 2, 3, 4, 5, 6, 7

[55] Wenshan Wang, Delong Zhu, Xiangwei Wang, Yaoyu Hu, Yuheng Qiu, Chen Wang, Yafei Hu, Ashish Kapoor, and Sebastian Scherer. Tartanair: A dataset to push the limits of visual slam. In *2020 IEEE/RSJ International Conference on Intelligent Robots and Systems (IROS)*, pages 4909–4916. IEEE, 2020. 6

[56] Yifan Wang, Jianjun Zhou, Haoyi Zhu, Wenzheng Chang, Yang Zhou, Zizun Li, Junyi Chen, Jiangmiao Pang, Chunhua Shen, and Tong He. π^3 : Scalable permutation-equivariant visual geometry learning, 2025. 3

[57] Andreas Wedel and Daniel Cremers. *Stereo scene flow for 3D motion analysis*. Springer Science & Business Media, 2011. 2

[58] Andreas Wedel, Clemens Rabe, Tobi Vaudrey, Thomas Brox, Uwe Franke, and Daniel Cremers. Efficient dense scene flow from sparse or dense stereo data. In *European conference on computer vision*, pages 739–751. Springer, 2008. 2

[59] Philippe Weinzaepfel, Thomas Lucas, Vincent Leroy, Yohann Cabon, Vaibhav Arora, Romain Brégier, Gabriela Csurka, Leonid Antsfeld, Boris Chidlovskii, and Jérôme Revaud. CroCo v2: Improved cross-view completion pre-training for stereo matching and optical flow. In *ICCV*, 2023. 6

[60] Weinzaepfel, Philippe and Leroy, Vincent and Lucas, Thomas and Brégier, Romain and Cabon, Yohann and Arora, Vaibhav and Antsfeld, Leonid and Chidlovskii, Boris and Csurka, Gabriela and Revaud Jérôme. CroCo: Self-supervised pre-training for 3D vision tasks by cross-view completion. In *NeurIPS*, 2022. 6

[61] Hongchi Xia, Yang Fu, Sifei Liu, and Xiaolong Wang. Rgbd objects in the wild: Scaling real-world 3d object learning from rgbd videos. In *Proceedings of the IEEE/CVF Conference on Computer Vision and Pattern Recognition*, pages 22378–22389, 2024. 6

[62] Yuxi Xiao, Qianqian Wang, Shangzhan Zhang, Nan Xue, Sida Peng, Yujun Shen, and Xiaowei Zhou. Spatialtracker: Tracking any 2d pixels in 3d space. In *Proceedings of the IEEE/CVF Conference on Computer Vision and Pattern Recognition*, pages 20406–20417, 2024. 7

[63] Yuxi Xiao, Jianyuan Wang, Nan Xue, Nikita Karaev, Yuri Makarov, Bingyi Kang, Xing Zhu, Hujun Bao, Yujun Shen, and Xiaowei Zhou. Spatialtrackerv2: 3d point tracking made easy. In *Proceedings of the IEEE/CVF International Conference on Computer Vision*, 2025. 3

[64] Jianing Yang, Alexander Sax, Kevin J. Liang, Mikael Henaff, Hao Tang, Ang Cao, Joyce Chai, Franziska Meier, and Matt Feiszli. Fast3r: Towards 3d reconstruction of 1000+ images in one forward pass. In *Proceedings of the IEEE/CVF Conference on Computer Vision and Pattern Recognition (CVPR)*, 2025. 3

[65] Yao Yao, Zixin Luo, Shiwei Li, Jingyang Zhang, Yufan Ren, Lei Zhou, Tian Fang, and Long Quan. Blendedmvs: A large-scale dataset for generalized multi-view stereo networks. In *Proceedings of the IEEE/CVF conference on computer vision and pattern recognition*, pages 1790–1799, 2020. 6

[66] Chandan Yeshwanth, Yueh-Cheng Liu, Matthias Nießner, and Angela Dai. Scannet++: A high-fidelity dataset of 3d indoor scenes. In *Proceedings of the IEEE/CVF International Conference on Computer Vision*, pages 12–22, 2023. 6

[67] Bowei Zhang, Lei Ke, Adam W Harley, and Katerina Fragkiadaki. Tapip3d: Tracking any point in persistent 3d geometry. In *The Thirty-ninth Annual Conference on Neural Information Processing Systems*, 2025. 3

[68] Chuhan Zhang, Guillaume Le Moing, Skanda Koppula, Ignacio Rocco, Liliane Momeni, Junyu Xie, Shuyang Sun, Rahul Sukthankar, Joëlle K Barral, Raia Hadsell, et al. Efficiently reconstructing dynamic scenes one d4rt at a time. *arXiv preprint arXiv:2512.08924*, 2025. 3

[69] Junyi Zhang, Charles Herrmann, Junhwa Hur, Varun Jampani, Trevor Darrell, Forrester Cole, Deqing Sun, and Ming-Hsuan Yang. MonST3R: A simple approach for estimating geometry in the presence of motion. In *ICLR*, 2025. 3, 4, 6, 7

[70] Songyan Zhang, Yongtao Ge, Jinyuan Tian, Guangkai Xu, Hao Chen, Chen Lv, and Chunhua Shen. Pomato: Marrying

pointmap matching with temporal motion for dynamic 3d reconstruction. In *Proceedings of the IEEE/CVF International Conference on Computer Vision*, 2025. 2, 3, 4, 7

[71] Zhoutong Zhang, Forrester Cole, Zhengqi Li, Michael Rubinstein, Noah Snavely, and William T Freeman. Structure and motion from casual videos. In *European Conference on Computer Vision*, pages 20–37. Springer, 2022. 3

[72] Yang Zheng, Adam W Harley, Bokui Shen, Gordon Wetzstein, and Leonidas J Guibas. Pointodyssey: A large-scale synthetic dataset for long-term point tracking. In *Proceedings of the IEEE/CVF International Conference on Computer Vision*, pages 19855–19865, 2023. 6

[73] Kaichen Zhou, Yuhang Wang, Grace Chen, Xinhai Chang, Gaspard Beaudouin, Fangneng Zhan, Paul Pu Liang, and Mengyu Wang. Page-4d: Disentangled pose and geometry estimation for 4d perception. *arXiv preprint arXiv:2510.17568*, 2025. 3

[74] Yang Zhou, Yifan Wang, Jianjun Zhou, Wenzheng Chang, Haoyu Guo, Zizun Li, Kaijing Ma, Xinyue Li, Yating Wang, Haoyi Zhu, Mingyu Liu, Dingning Liu, Jiange Yang, Zhoujie Fu, Junyi Chen, Chunhua Shen, Jiangmiao Pang, Kaipeng Zhang, and Tong He. Omniworld: A multi-domain and multi-modal dataset for 4d world modeling, 2025. 6

[75] Dong Zhuo, Wenzhao Zheng, Jiahe Guo, Yuqi Wu, Jie Zhou, and Jiwen Lu. Streaming 4d visual geometry transformer. In *The Thirteenth International Conference on Learning Representations*, 2026. 3

A. Appendix

Table 4. Key training hyperparameters.

Setting	Stage 1	Stage 2
Epochs	100	100
Resolution	224	512
Pairs per epoch	900K	84K
Batch size	256	64
Warmup epochs	10	20
Peak learning rate	1e-4	
Final learning rate	1e-6	
Optimizer	Adam	
LR schedule	linear warmup + cosine decay	
Gradient clipping	max norm 10	

Table 5. Summary of notations.

Symbol	Meaning
	Input
$\mathbf{I} \in \mathbb{R}^{H \times W \times 3}$	input image
$\mathbf{I}' \in \mathbb{R}^{H \times W \times 3}$	the other input image
	Output
$\mathbf{P} \in \mathbb{R}^{H \times W \times 3}$	point position map for \mathbf{I}
$\mathbf{F} \in \mathbb{R}^{H \times W \times 3}$	scene flow map for \mathbf{I}
$\mathbf{W} \in \mathbb{R}^{H \times W}$	pose weight map for \mathbf{I}
$\mathbf{C} \in \mathbb{R}^{H \times W}$	confidence map for \mathbf{I}
	Derived
$\hat{\mathbf{T}} \in \mathbb{R}^{3 \times 4}$	solved rigid transformation of \mathbf{I} relative to \mathbf{I}'
$i \in \mathbb{N}$	pixel index
$\mathbf{P}^i \in \mathbb{R}^3$	point position for pixel i in \mathbf{I}
$\mathbf{P}_v^i \in \mathbb{R}^3$	\mathbf{P}^i in the view of \mathbf{I}'
$\mathbf{P}_t^i \in \mathbb{R}^3$	\mathbf{P}^i at the timestamp of \mathbf{I}'
$\mathbf{P}_{vt}^i \in \mathbb{R}^3$	\mathbf{P}^i in the view and at the timestamp of \mathbf{I}'
$\mathbf{F}^i \in \mathbb{R}^3$	scene flow for pixel i in \mathbf{I} towards \mathbf{I}'
$\mathbf{F}_v^i \in \mathbb{R}^3$	rigid component (camera motion) of \mathbf{F}^i
$\mathbf{F}_t^i \in \mathbb{R}^3$	non-rigid component (object motion) of \mathbf{F}^i
$f \in \mathbb{R}^+$	focal length (assumed identical on both axes)
$\mathbf{c} \in \mathbb{R}^2$	optical center of the camera
$\mathbf{p} \in \mathbb{R}^{H \times W \times 2}$	projected point position map for \mathbf{I}
$\mathbf{f} \in \mathbb{R}^{H \times W \times 2}$	optical flow map for \mathbf{I}